



# Detecting high and low-intensity fires in Alaska using VIIRS I-band data: An improved operational approach for high latitudes



Christine F. Waigl<sup>a,\*</sup>, Martin Stuefer<sup>a</sup>, Anupma Prakash<sup>a</sup>, Charles Ichoku<sup>b</sup>

<sup>a</sup> Geophysical Institute, University of Alaska Fairbanks, Fairbanks, AK, USA

<sup>b</sup> Climate & Radiation Laboratory (Code 613), NASA Goddard Space Flight Center, Greenbelt, MD, USA

## ARTICLE INFO

### Article history:

Received 23 November 2016

Received in revised form 12 May 2017

Accepted 7 July 2017

Available online 4 August 2017

### Keywords:

Active fire detection

S-NPP/VIIRS

MODIS

Boreal forest fire

High- and low-intensity active fires

Alaska

## ABSTRACT

Fire products from Moderate Resolution Imaging Spectroradiometer (MODIS) and Visible Infrared Imaging Radiometer Suite (VIIRS) imagery provide timely information for wildfire detection, monitoring, and characterization at the global scale. However, in Alaskan boreal forest fires, their lower effectiveness in detecting residual fire once the high-intensity fire front has passed limits their practical use for regional or local fire management decisions. Using data acquired during Alaska's 2016 fire season, we analyzed the performance of the MODIS-based MOD14/MYD14, and the more recent VIIRS I-band active fire products. A comparison with the fire perimeter and properties data published by the Alaska Interagency Coordination Center (AICC) shows that both MODIS and VIIRS fire products successfully detect all fires larger than approximately 200–300 ha. For fires smaller than this threshold, the VIIRS I-band product offers higher detection likelihood. To map burn areas containing both low- and high-intensity active fire, we developed the VIIRS I-band Fire Detection Algorithm for High Latitudes (VIFDAHL). We apply this algorithm to regions of known Alaskan boreal forest fires and validate it using events mapped by fire management agencies and detected on closely-timed Landsat imagery. We find that for Alaska, an example of a high-latitude region, VIFDAHL more accurately captures the fire spread, can differentiate well between low- and high-intensity fires, and can detect 30–90% more fire pixels compared to the MODIS and VIIRS global fire products.

© 2017 Elsevier Inc. All rights reserved.

## 1. Introduction

Operational fire detection products from satellite-borne visible and infrared sensors have been used to track wildfire activity and inform fire managers of fire risk and hazard since they first became available in the 1980s (Ichoku et al., 2012). In the northern high-latitude regions such as Alaska, where fire affects remote, sparsely populated areas, site access or fire suppression decisions are associated with significant complexity and cost. In such areas, satellite remote sensing frequently offers the only avenue to obtain near real-time data for decision support.

In Alaska's vast boreal forest, wildfires have been reported to be increasing in frequency, severity, and extent, in part due to a rapidly changing climate regime (Kasischke and Turetsky, 2006; Soja et al., 2007; Collins et al., 2013). Between 1960 and 2000, the area annually affected by fire increased from an average of 400,000 ha per year to approx. 767,000 ha per year (Kasischke et al., 2010). In the Alaskan boreal forest, stands of black spruce (*Picea mariana*), the dominant

coniferous species, undergo a complete stand-replacing fire roughly every 50–500 years (Kasischke et al., 2010). Due to the slow progress of decomposition in the sub-arctic climate a deep layer of fine organic material covers the forest floor. The combustion of this duff layer accounts for more than half of the fire-related carbon consumption and emissions in boreal forest areas (Kasischke et al., 2005; Randerson et al., 2006; Kasischke and Hoy, 2012); the degree to which it is consumed impacts carbon storage (Genet et al., 2013) and the succession of species during post-fire recovery (Johnstone et al., 2010). Rapid changes in the frequency and characteristics of Alaskan wildfires therefore affect the atmospheric composition at local (Grell et al., 2011; Andreae and Merlet, 2001) and hemispheric scales (Pfister et al., 2005, 2006, 2008). The investigation of some of these processes requires observational data to be available in near real time.

In 2015 Alaska witnessed an extreme fire season, with the total area burned exceeding 2.5 million ha (Roman, 2015), which is six times the long-term annual average. Since the start of the Alaska Large Fires Database in 1940 (Kasischke et al., 2002) the area burned in 2015 was only exceeded during the 2004 fire season. 2015 was followed by a below-average fire season in 2016 (200,000 ha burned). These two recent fire seasons provide an excellent opportunity to investigate a variety

\* Corresponding author at: Geophysical Institute, 903 Koyukuk Drive, University of Alaska, Fairbanks, AK 99775-7320, USA.

E-mail address: [cwaigl@alaska.edu](mailto:cwaigl@alaska.edu) (C.F. Waigl).

of fires that are representative for the fire regime in the Alaskan boreal forest.

The goals of this study are to use 2015 and 2016 data as a test case:

- To investigate the performance of the principal fire products currently available for operational use in the detection and mapping of Alaskan wildfires, using fire properties and perimeter data provided by fire management agencies as reference data.
- To design and evaluate a customized fire detection algorithm suitable for Alaska and to compare its performance to the global product as well as validate it with higher-resolution data.

We first provide a brief review of existing global fire detection products, introduce four study sites, and evaluate selected global fire products with ground truth data available from fire management agencies. We then present the VIIRS I-band Fire Detection Algorithm for High Latitudes (VIFDAHL), validate it using higher-resolution remote sensing data, and compare its performance with the previously evaluated global fire products.

## 2. Global active fire products: a brief review

Most global operational fire products make use of two infrared (IR) bands: one in the mid-IR (centered at a wavelength of  $\sim 4 \mu\text{m}$ ), which corresponds to the peak of radiant emittance caused by a flaming wildfire at  $\sim 1000 \text{ K}$ ; and a second band in the thermal IR (at  $\sim 11\text{--}12 \mu\text{m}$ ), which is sensitive to background radiation emitted by the Earth's surface. Whenever a pixel's footprint covers the location of a wildfire, the mid-IR radiance is elevated with respect to the thermal IR radiance. Fire detection algorithms use thresholds on both the value of the mid-IR emissive signal and the difference between the mid- and thermal IR brightness temperatures. Algorithm-dependent checks serve to minimize errors of commission ("false alarms") and errors of omission ("missing fire pixels").

The Wildfire Automated Biomass Burning Algorithm (WF-ABBA), developed for fire retrieval from Geostationary Operational Environmental Satellite (GOES) and other geostationary satellites operated by European, Japanese and Korean agencies, was used to generate an operational fire detection product with a spatial resolution of 4 km at the equator as early as 1994 (Prins and Menzel, 1994; Menzel and Prins, 1996; Prins and Schmidt, 2001). However, it was only in 2002 that a WF-ABBA based daily fire product was available operationally for the user community through NOAA's National Environmental Satellite, Data, and Information Service (NESDIS). Sub-pixel analysis is used to retrieve the temperature and the fractional areas of fires in individual pixels (Dozier, 1981; Matson and Dozier, 1981).

A family of fire detection algorithms was also developed for the Advanced Very High Resolution Radiometer (AVHRR) on NOAA's polar-orbiting satellites (Giglio et al., 1999; Li et al., 2000a; Li et al., 2000b). The Fire Identification, Mapping and Monitoring Algorithm (FIMMA), which is available at NESDIS, is specifically aimed at the detection of forest fires, as it relies on land cover data among its inputs to complement the AVHRR bands 2 ( $0.9 \mu\text{m}$ ), 3b ( $3.7 \mu\text{m}$ ), 4 ( $10.8 \mu\text{m}$ ) and 5 ( $12 \mu\text{m}$ ) that are used.

Following the launch of the National Aeronautics and Space Administration's (NASA's) Earth Observing System (EOS) suite of satellites beginning in 1999, the Moderate Resolution Imaging Spectroradiometer (MODIS) sensors offered new opportunities for advancing fire detection and characterization. MODIS data are used to generate the currently best-validated active fire detection products, MOD14 and MYD14 (from the Terra and Aqua spacecraft, respectively), at a spatial resolution of 1 km at nadir (Kaufman et al., 1998; Justice et al., 2002). Originally described by Kaufman et al. (1998), the MODIS operational algorithm version has since evolved from collections 2, 3, 4, and 5 (Giglio et al., 2003) up to the current

collection 6 (Giglio et al., 2016). MODIS acquires data in 36 spectral bands, ranging from visible and near infrared (VNIR) to short-wave infrared (SWIR), mid-infrared (MIR) and thermal infrared (TIR). 29 of the 36 spectral bands are acquired at a ground-sampling distance (GSD) of 1 km at nadir. Off-nadir, pixel footprints grow to up to approximately  $2 \times 5 \text{ km}$  at the swath edge. Active fire detection makes use of two channels centered at  $3.96 \mu\text{m}$  (band 21 and the more sensitive band 22, which saturates at a lower brightness temperature) and the TIR channel 31, which is centered at  $11 \mu\text{m}$ .

The Visible Infrared Radiometer Suite (VIIRS) on the National Oceanic and Atmospheric Administration's (NOAA's) Suomi National Polar-orbiting Partnership (Suomi NPP) platform (Cao et al., 2014) was launched in late 2011 under the Joint Polar Satellite System (JPSS), which is a joint program managed by both NOAA and NASA. A fire detection algorithm based on the moderate-resolution ("M") bands (GSD 750 m at nadir) uses the dual-gain band M13 ( $3.973\text{--}4.128 \mu\text{m}$ , with saturation temperatures of 343 K and 634 K) and the single-gain band M15 ( $10.263\text{--}11.263 \mu\text{m}$ ) (Csiszar et al., 2014). A second algorithm, devised by Schroeder et al. (2014) uses the bands optimized for imaging ("I" bands, GSD 375 m at nadir), specifically I4 (centered at  $3.74 \mu\text{m}$ ) and I5 (centered at  $10.45 \mu\text{m}$ ). Polivka et al. (2016) have proposed the Firelight Detection Algorithm (FILDA), which combines VIIRS M-band infrared data with the visible light signal from the near-constant contrast Day-Night Band (DNB) (Liang et al., 2014) for improved night-time fire detection.

Csiszar et al. (2006) validated the MODIS active fire products using simultaneous higher-resolution data from the Advanced Spaceborne Thermal Emission and Reflection Radiometer (ASTER) on the Terra platform for wildfires in the Eurasian boreal forest in Siberia. They found that, due to the thick smoke observed in Siberian boreal forest fires, the footprint of a  $1 \times 2 \text{ km}$  MODIS pixel needs to contain one third more 30 m ASTER fire detections than required for fires in the Brazilian Amazon (60 vs. 45) to achieve a probability of 50% for the pixel to be flagged as "fire". Schroeder et al. (2008) validated WF-ABBA and the MODIS products using ASTER and Landsat ETM+ over Amazonia. A different approach to validation consists in the comparison of the output from newer products to existing ones. Thus, Schroeder et al. (2014) compared the new VIIRS 375 m I-band global product to MOD14/MYD14 and to the VIIRS M-band product, by sampling 12 zones across the globe for one month (August 2013). Two of these zones are in the boreal region, one over Canada, one over Russia. For these zones, errors of commission do not exceed 0.04% (Schroeder et al., 2014). Direct comparison with MODIS as well as higher-resolution sensors was carried out for fire events in California, Brazil, and Australia, but no locations in the boreal forest were selected for detailed investigation.

## 3. Wildfire study areas

In this study we use four selected study sites (Fig. 1) to generate and validate a new Alaska-specific VIIRS I-band based fire product. They represent distinct situations in which fire was active during the 2015 or 2016 Alaska fire seasons. For these sites, cloud-free Landsat 8 Operational Land Imager (OLI) data that was closely timed with one of the VIIRS overpasses in our dataset was available.

### 3.1. Willow: Sockeye fire, June 2015

A human-caused wildfire started on the northern outskirts of the town of Willow, southcentral Alaska, on June 14, 2015. High winds and dry weather conditions caused the fire to rapidly grow and spread southwards. Numerous buildings were destroyed. The area north of Willow consists mainly of mature black spruce forest, interspersed by birch and balsam poplar and bordered by alluvial plains covered in grass and brush. The Susitna River borders the area in the west.

Unlike most Alaskan boreal forest fires, the road-accessible Sockeye fire was vigorously suppressed. Thus, significant flaming fire activity

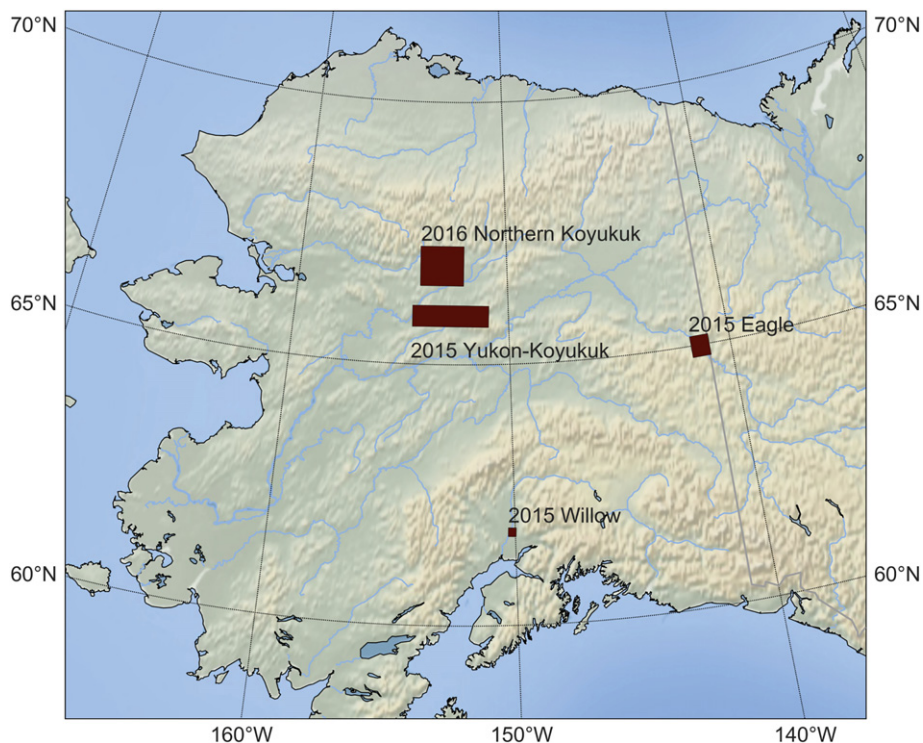


**Fig. 1.** Location of the four 2015 and 2016 wildfire study areas within Alaska: Willow (Sockeye fire), Eagle (Seventymile and Trout fire), and two areas within the northern Yukon-Koyukuk basin which saw multiple large-scale and high intensity wildland fire events during both July 2015 and 2016.

was limited to less than one week. We selected this fire site as it offers a diversity of surface characteristics and fuels that were likely to cause false positive detections in the new Alaska-specific algorithm. This is due to the extensive bare, dry, highly reflective sand banks along the Susitna river as well as an old fire scar in the vicinity. Cloud cover also varied widely throughout the active phase of this fire event.

The geographic extent of this study area is latitude 61.7–61.9°N, longitude 150.0–150.1°W.

### 3.2. Yukon-Koyukuk: multiple wildfires, July 2015

During the last third of the month of June 2015, with hot, dry, windy weather continuing in western interior Alaska, multiple wildfires were ignited by lightning across the rural areas of northern Yukon-Koyukuk region. These fires offer an excellent test case for fire detection and mapping, in particular for large-scale, high-intensity burns in a remote area with little infrastructure and predominately black spruce forest. We include the following large fire events: Sushgitit Hills (discovered June 21, final area 126,633.5 ha), Rock (June 19, 57,728.6 ha), Torment Creek (June 20, 33,359.1 ha), Tobatokh (June 22, 21,867.6 ha), and Holonada (June 22, 19,496.2 ha). Detections from neighboring fire perimeters that were active at the same time (Banddana Creek and Isahultila) are sometimes present at the edge of the study area. The fires remained active from the time of ignition to mid-August, when wet weather ended large-scale wildfire activity.

We selected this site because the fire events generated a large amount of data (>1000 detections in a single acquisition), with high fire intensity, and abundant smoke and clouds. As the area is remote and sparsely populated the fires were classified in the “limited” management option by the fire protection agencies and essentially left unsuppressed. The only exception is the Rock fire, in the “full” management option, due to its proximity to the village of Hughes on the banks of the Koyukuk River. The VIIRS data for this area contain numerous test cases for data anomalies due to sensor saturation and intense signals.

The geographic extent of this study area is latitude 65.75–66.1°N, longitude 150.9–154.5°W.

### 3.3. Eagle: early-season wildfires, May 2015

We further selected a small area north of the town of Eagle, AK, which was affected by early-season lightning-ignited fires in late May 2015. The area is mountainous, largely covered by either black spruce forest or alpine tundra interspersed with rocky outcrops. The Seventymile fire (1175 ha) was located approximately 10 km northwest of Eagle, and the Trout fire (106.7 ha) was a smaller nearby event.

The geographic extent of this study area is latitude 64.75–65.17°N, longitude 140.95–141.75°W.

### 3.4. Northern Koyukuk: multiple large fires, July 2016

From the 2016 fire season we selected a study area containing several of the largest fires of 2016, during a short period of particularly intense fire activity: Hog (discovered July 5, 23,700.5 ha), Hogaza River (June 26, 21,179.1 ha), Iniakuk Lake (June 25, 14,872.0 ha) and Bedrock Creek (July 3, 2650 ha).

The geographic extent of this study area is latitude 66.5–67.25°N, longitude 152.1–154.2°W.

## 4. Data

This study required data from the northern high latitudes. While on the one hand overlapping tracks of polar orbiting satellites provide more coverage (and thus more frequent data) in higher latitudes, poorer computer network infrastructure still poses challenges for reliable and quick data transmission from mid-latitudes to higher-latitude areas for near-real time applications. However, local data downlink stations in the high latitudes provide an opportunity to overcome this challenge. Even though this work is based on data from NOAA and NASA data repositories, it was undertaken with a view towards future operational use based on processing locally downlinked data to detect and map fires, and tailor the fire products to regional and local needs.

#### 4.1. Global MODIS and VIIRS I-band products

We downloaded MODIS and VIIRS I-band fire detection data from the Land, Atmosphere Near real-time (NRT) Capability for EOS (LANCE) system, specifically the Fire Information for Resource Management System (FIRMS) [<https://earthdata.nasa.gov/firms>]: The near real-time VIIRS 375 m I-band Active Fire product VNP14IMG1 (DOI:<http://dx.doi.org/10.5067/FIRMS/VIIRS/VNP14IMG1.NRT.001>) and the MODIS Collection 6 NRT Hotspot/Active Fire Detections MCD14DL (DOI:<http://dx.doi.org/10.5067/FIRMS/MODIS/MCD14DL.NRT.006>). At the time of writing, availability of the VIIRS 375 m I-band product via NASA's portals begins in January 2016. Therefore, we used the 2016 fire season for the evaluation of global fire products. After limiting the data to the geographic extent of the Alaska, the dataset contained:

- MODIS (based on MODIS Terra and Aqua): 3769 detected hotspots
- VIIRS I-band (375 m, based on VIIRS on Suomi NPP): 11,091 detected hotspots.

Each data record represents the latitude and longitude of a fire detection associated with the following attributes: timestamp and brightness temperature measurements, the along-scan and along-track linear extent of the fire pixel's footprint on the ground, a confidence index, and fire radiative power.

Regarding the three 2015 study areas, we were also able to obtain NASA-processed VIIRS 375 m I-band active fire data for selected days in 2015, courtesy Wilfrid Schroeder (University of Maryland and NOAA/NESDIS Center for Satellite Applications and Research).

#### 4.2. VIIRS Sensor Data Record (SDR) data

We based the design of an Alaska-specific VIIRS I-band fire detection algorithm on VIIRS at-sensor brightness temperature swath data. For this study, we used VIIRS Sensor Data Record (SDR) data from NOAA's Comprehensive Large Array-data Stewardship System (CLASS) data portal. Throughout the entire active fire phase of our two smaller study areas (Willow and Eagle), all available VIIRS SDR datasets, with the exception of those dominated by cloud cover or lacking any active fire, were analyzed. For the large-scale study areas (Yukon-Koyukuk and Northern Koyukuk), the analysis is based on the one or two VIIRS scenes that coincide with the available Landsat 8 data. For later operational use, locally downlinked and processed data from the Geographic Information Network of Alaska (GINA) at the University of Alaska Fairbanks (UAF), a data provider that operates an X-band direct read-out station, will be available. VIIRS SDR data is provided as HDF5 data files aggregating multiple bands and 86-second granules, plus terrain-corrected geodata layers for each granule and each sensor band group (I-bands, M-bands and Day-Night-Band).

The swath acquired by VIIRS is 3040 km wide, 30% wider than a MODIS swath (2330 km). The Suomi NPP orbit closely follows that of Aqua (in the "A-train"), but at an orbit that is >100 km higher. Like Aqua, Suomi NPP makes early afternoon overpasses on an ascending node each day. The repeat interval is 16 days, the same as Aqua and Terra, so orbital tracks vary from day to day. At a minimum, two good daytime and two good nighttime overpasses can be expected daily for any location in interior Alaska.

#### 4.3. Fire location and perimeter data

To evaluate the fire detections against a measure for "true" fires, we used the 2016 (and, limited to the study areas, 2015) additions to the Alaska Large Fires Database (ALFD) (Kasischke et al., 2002) from the AICC's Geographic Information System (GIS) portal (<http://afsmaps.blm.gov/imf/imf.jsp?site=firehistory>). The 2016 dataset consists of a Shapefile containing 155 fire perimeters, in a geographic coordinate

system using the NAD83 datum. AICC also distributes an additional "Fire Locations" file, which provides point data for the initial location of all events managed by AICC during the fire season; this is a superset of the fires in the ALFD. For 2016, after removing events marked as false alarms, there are 592 such fire locations. The GIS files are updated approximately daily during the fire season; they were retrieved in their final form in 2017, after the 2016 season ended.

The attribute information (Table 2) published by the AICC includes dates (first detection, last management action, date the fire was confirmed "out"), environmental factors (fire cause, primary fuel, total burned area in acres) and management related information, such as false-alarm flags. During pre-processing we confirmed that none of the 155 fires from the ALFD are marked as false alarms. Inspection of the fire events without corresponding fire perimeter shows that such fires are typically very small (<1 ha) human-caused fires, often in residential or industrial areas, and that data available for them may be incomplete. Given our interest in wildland fires we only analyzed fires for which a perimeter is available, that is, the 155 ALFD fire events.

During the active management phase of a fire event, operational fire detections from VIIRS and MODIS are among the data sources used to update fire perimeter geometries. However, at the end of a fire event the final perimeter data is corrected using the best available source, such as aerial GPS surveys or digitization of Landsat fire scar imagery (Jennifer Jenkins, Alaska Fire Service GIS manager, personal communication). In the 2016 data, 66 final perimeters (43%) were generated from Landsat 8 imagery, 16 (10%) from aerial survey data, 34 (22%) were provided by operational teams affiliated with the Alaska Department of Forestry or the National Park Service, 26 (17%) from various operational sources, and 13 (8%) were lacking provenance information. Out of the 10 largest fires, 8 perimeters relied on Landsat 8 data.

2016 fire areas range from 0.2 ha to 23,700.5 ha, with a mean of 1293.7 ha and a median of 83.5 ha. Six fire events exceeded 10,000 ha. The 2016 fire season was below-average, with many relatively small fires. As a point of comparison, for the extreme 2015 fire season we count 334 fire perimeters with a mean area of 6236.2 ha, a median of 1128.5 ha and a maximum of 126,633.5 ha. 133 out of 155 2016 fire events (86%) were labeled as caused by lightning, compared to only 22 (14%) human-caused fires. Typically, only few large wildland fires are caused by human action in interior Alaska. To be able to compare and measure distances, we re-projected the geospatial coordinate information in the fire events and the fire detection datasets to the Alaska Albers Equal Area projection.

#### 4.4. Landsat 8 imagery

To validate the Alaska-specific VIIRS fire detection algorithm, we used three Landsat 8 OLI images that were acquired within minutes of an available VIIRS granule of the same location (Table 3). For the 2016 Northern Koyukuk study area, for which the time lapse between Landsat and the two closest VIIRS overpass times is approximately 45 min and 58 min, respectively, Landsat fire detections were not suitable to validate VIIRS-based detections and are therefore used for visualization purposes only.

### 5. Methods

#### 5.1. Evaluation of operational MODIS and VIIRS I-band products

For each of the 155 ALFD fires we counted the hotspot detections that are located within a buffer of 1 pixel (at nadir) around the fire perimeter: 375 m for VIIRS and 1 km for MODIS data. Furthermore, we required detection time stamps to fall between the "discovery date" and either the "out date" or, if unavailable, the "control date" attributes of the fire event. The buffer was used to ensure that fire pixels whose centers lie just outside the recorded perimeter are correctly counted. The

footprint of a MODIS fire pixel is 1 × 1 km at nadir, but can become stretched to a maximum of 2 × 5 km at the swath edge. VIIRS I-band pixels are nearly square with a side of 375 m, and grow by a factor approximately 2 towards the swath edge. The resulting dataset was then statistically analyzed to compare the performance of VIIRS I-band and MODIS hotspot counts and to evaluate their spatio-temporal distribution.

5.2. VIIRS I-band Fire Detection Algorithm for High Latitudes (VIFDAHL)

Our processing scheme ingests VIIRS data that are processed to the SDR processing level (Fig. 2); it is based on the following design goals:

- all fire pixels correctly detected by the global VIIRS I-band product must also be detected by VIFDAHL

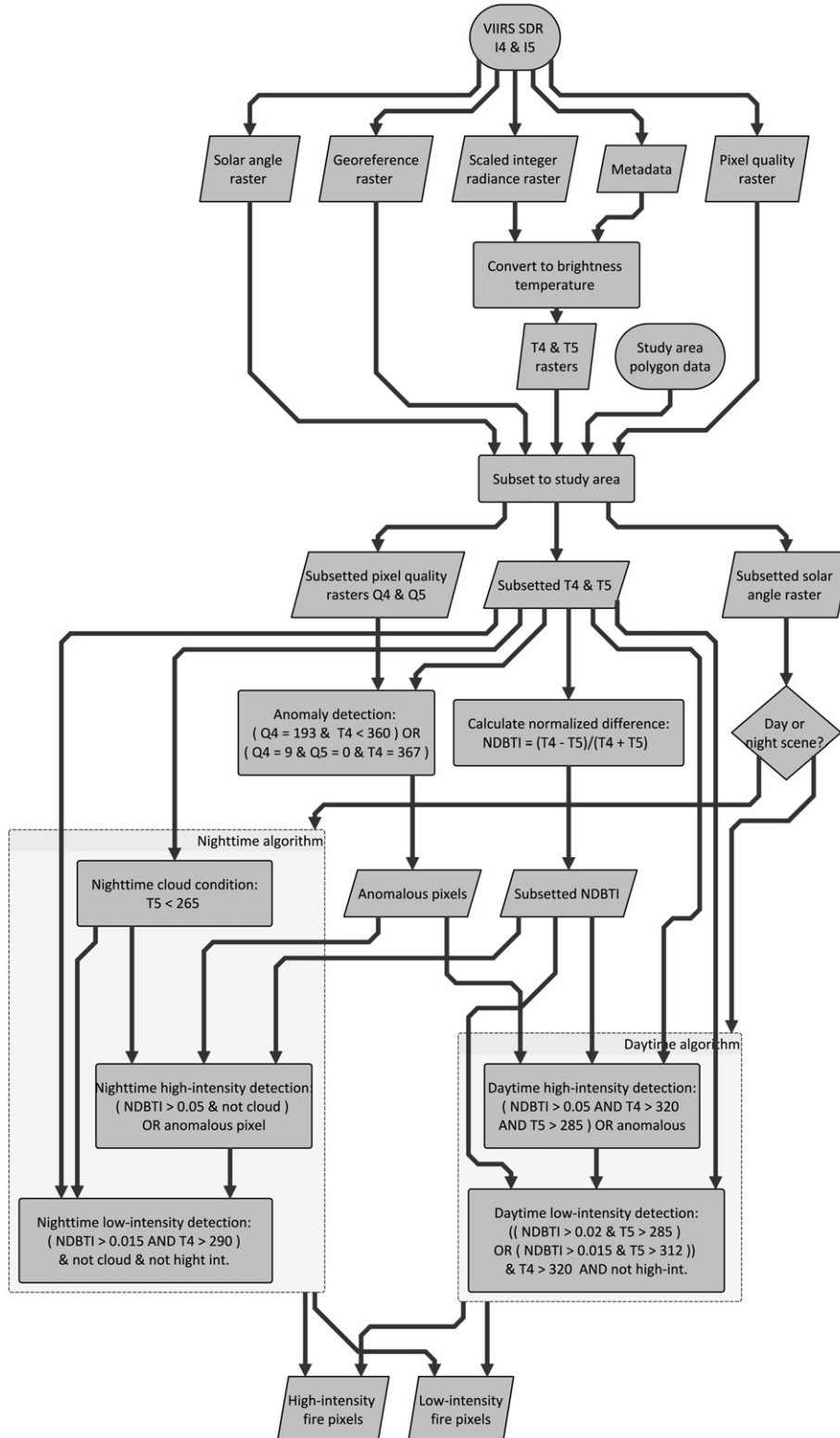


Fig. 2. VIFDAHL (VIIRS I-band Fire Detection Algorithm for High Latitudes) processing workflow.

- saturated pixels due to fire-related radiance are detected as fire
- the product is superior to the global VIIRS I-band product in detecting residual fire behind the fire front
- fire detections are classified into high- and low-intensity fire pixels
- false-detection filters are optimized for sources typically found in Alaska, specifically sand banks and old fire scars
- duplicate detections due to the bowtie effect are removed.

We generate the resulting detection product as a polygon vector data in order to preserve the extent of the pixel footprint.

The scaled integer data in bands I4 (centered at 3.74  $\mu\text{m}$ ) and I5 (11.45  $\mu\text{m}$ ) were converted to at-sensor brightness temperature T4 and T5 (Schroeder et al., 2014). As in other fire detection algorithms, VIFDAHL relies on a large difference in the I4 and I5 brightness temperatures (T4, T5); pixels that have no elevated T4 or appear cold in T5 (cloud, water) are discarded. In order to remove highly reflective riverbanks, we need the thermal signal to be elevated as well. To ensure that thresholds apply across meteorological conditions, we calculate a Normalized Difference Brightness Temperature Index (NDBTI):

$$\text{NDBTI} = \frac{T4 - T5}{T4 + T5}$$

NDBTI values for a typical active fire are shown in Fig. 3: Fire pixels show elevated NDBTI values, with the active fire front clearly distinguished from residual fire within the fire perimeter. Potential sources of false detections are the sandy banks of the river visible to the left of the fire and an eight year old fire scar in the top left corner. We used a minimum in the NDBTI frequency distribution close to 0.05 to delineate low- and high-intensity fire areas. Due to the risk of false detections in

locations that are in reality highly-reflective river banks, we added a check for elevated T5 (>312 K) for daytime images. The thresholds for absolute values of T5 and T4 have been fixed via a grid search and sampling across the test scenes (Table 1): we maximized the detections within the known fire perimeter up to the point where false detections started to appear in the known non-fire areas. For each test scene, the entire VIIRS swath, subsetted to the extent of Alaska, was checked for false detections not associated with a known fire.

A further consideration relates to artifact conditions associated with fires. To assess them, we considered the pixel quality rasters for both band 4 and band 5 (Stevens, 2014). These are 1-byte raster bands of the same extent and pixel geometry as their respective radiance swaths. The single byte encodes four separate 2-bit quality flags for each pixel as shown in Table 4. For nominal data, the value 0 (= 00|00|00|00) would be expected.

In the Yukon-Koyukuk study area we found the following anomalous pixel quality values:

- **2** = 00|00|00|10 (“no calibration”) in both bands I4 and I5. These are essentially no-data pixels, located towards swath edge, and represent bowtie removal.
- **9** = 00|00|10|01 in band I4: “poor calibration, all saturated”
- **65** = 01|00|00|01 in band I5: “poor calibration radiance out of range”
- **193** = 11|00|00|01 in band I4: “poor calibration, radiance and reflectance out of range”.

As is the case for the wildfires in the contiguous United States examined by Schroeder et al. (2014), the T4 brightness temperature associated with Q4 = 9 was at its maximum value (367 K), whereas Q4 = 193 indicates folded values caught at the lower end of the permissible data range (T4 = 208 K). In a small number of pixels we found Q5 = 65 associated with Q4 = 193 and a saturated T5 (see white arrows in Fig. 4). Whenever Q4 = 9 or Q4 = 193, the pixel is counted as a high intensity fire pixel by VIFDAHL, but the brightness temperature value for these pixels does not provide any meaningful information. Furthermore, Fig. 4 also shows some pixels appear dark in the T4 plot, for which T5 is elevated compared to background; but Q4 and Q5 are both zero (nominal quality, no green outline) even though T4 is potentially anomalous. VIFDAHL does not flag these ambiguous cases as fire pixels.

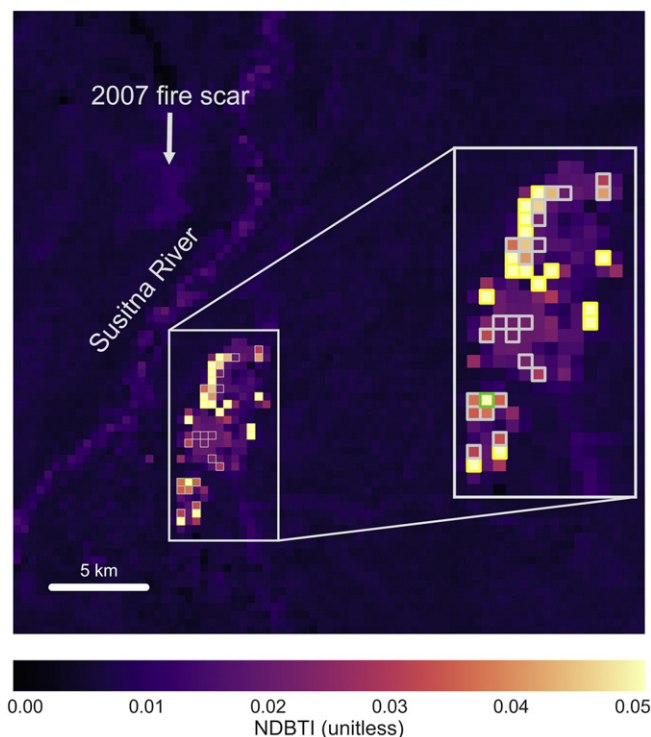


**Fig. 3.** Willow study area, Sockeye fire 2015-06-15, 15:09 AKDT: Normalized Difference Brightness Temperature Index (NDBTI) from VIIRS I-band data, overlaid with VIFDAHL detections: high-intensity (yellow outline), low-intensity (grey outline), saturated (green outline). VIFDAHL was tuned to avoid false positive detections along the sun-heated riverbanks of the Susitna as well as for the fire scar of the 2007 Su River fire, despite the elevated NDBTI values in these areas. The center of this scene is at latitude 61.84°N, longitude 150.1°W.

**Table 1**  
Overview of VIIRS swath data scenes that were used for each study area.

study area	# VIIRS SDR granules used	Start date	End date
Eagle	5	2015-05-27	2015-05-29
Willow	19	2015-06-14	2015-06-19
Yukon-Koyukuk	1	2015-07-06	2016-07-06
Northern Koyukuk	2	2016-07-15	2016-07-15

**Table 2**  
GIS attributes in the AICC and global fire product datasets that were used in this study. Attribute names are truncated from the names used within the AICC's database.

File	Field name	Description
AICC perimeters	CalcAcres	Final total area of the burn perimeter, in acres
	FireName	Name of fire (text label)
	DiscDate	Date on which fire was discovered (AKDT)
	ControlDate	Date on which fire was under control
	OutDate	Date on which fire was extinguished
	FalseAlarm	Flag marking false alarm fires
	GenCause	Fire cause (human or lightning)
	Comment	Plain text comment relating to the provenance of perimeter geometry data
	MODIS, VIIRS-I	ACQ_DATE
ACQ_TIME		Time of detection (UTC)

**Table 3**

Landsat and VIIRS scenes used for validation of the AK-specific VIIRS I-band fire detection scheme.

Landsat scene ID	Landsat date-time (UTC)	VIIRS orbit	VIIRS granule ID	VIIRS granule start time (UTC)	Study area
LC80650142015147LGN00	2015-05-27 20:47:22	18,565	NPP001135168656	2015-05-27 20:45	Eagle
LC80700172015166LGN00	2015-06-15 21:19:17	18,820	NPP001150756980	2015-06-15 21:28	Willow
LC80730142015187LGN00	2015-07-06 21:36:48	19,118	NPP001168905804	2015-07-06 21:36	Yukon-Koyukuk
LC80740132016197LGN00	2016-07-15 21:43:04	24,438	NPP001492885869	2016-07-15 20:58	Northern Koyukuk
		24,439	NPP001492947321	2016-07-15 22:41	

**Table 4**

VIIRS I-band pixel quality raster data key.

2 bits: calibrated pixel value outside look-up table limits	2 bits: data required for calibration missing	2 bits: level of pixel saturation	2 bits: calibration quality
00: all within range	00: no missing data	00: none saturated	00 good calibration
01: radiance out of range	01: Raw Data Record missing	01: some saturated	01 poor calibration
10: reflectance or brightness temperature out of range	10: calibration data missing	10: all saturated	10 no calibration
11: both out of range	11: thermistor data missing	11: not used	11 not used

### 5.3. Validation using Landsat 8

To validate VIFDAHL we used near-simultaneous Landsat 8 OLI imagery. We implemented the fire detection algorithm described in Schroeder et al. (2016), which uses spectral reflectance in the OLI SWIR bands (B5 and B7) to preselect “unambiguous” and “marginal” fire pixels and then re-examines the “marginal” pixels using contextual tests on the B7 reflectance and the B7/B5 reflectance ratio with a 61 by 61 pixel window.

## 6. Results

### 6.1. Exploratory data analysis of operational MODIS and VIIRS I-band fire detection datasets

Neither of the two global fire products is able to detect all 2016 ALFD wildfires: MODIS failed to detect 45% and the VIIRS 375 m I-band product failed to detect 35% of the fires. These relatively high percentages are due to the small size and short burn duration of most 2016 fires, and cloud conditions. As summarized in Table 5, the VIIRS I-band product detects more fires than the MODIS product, offers an improvement in the detection of smaller fires and detects numerous thermal anomalies that are not wildfire, but instead associated with the Prudhoe Bay oil fields on the North Slope of Alaska or volcanic eruptions in the Aleutian

arc. A small percentage of detections (2% for VIIRS, 3.3% for MODIS) remain unassigned to either an ALFD wildfire or another known source. Out of these unassigned detections, approximately 40% for VIIRS (85 out of 224) and half for MODIS (63 out of 126) are located within 5 km of a fire perimeter and are therefore likely to be associated with it. The remainder consists in a mix of industrial hotspot and sporadic detections of unknown origin, more commonly found for the more sensitive VIIRS.

The number of VIIRS I-band fire pixels per fire is generally greater than the number of MODIS pixels because of the much higher resolution of VIIRS I-band (375 m) relative to MODIS (1 km). The relationship is strongly linear ( $r^2 = 0.93$ , see Fig. 5), and there are on average 2.9 times the number of VIIRS detections for a fire event as MODIS detections (95% Confidence Interval (CI) for the slope: [2.83, 3.02]). There is a roughly linear relationship between a fire's size and the number of fire detections contained within it (Fig. 5). From linear regression we find an average of 1.63 MODIS detections (95% CI: [1.51, 1.74],  $r^2 = 0.84$ ) for each square kilometer of final area burned, and 4.66 VIIRS I-band detections ([4.26, 5.06],  $r^2 = 0.78$ ).

After early August, when rain inhibited the fire activity (Fig. 6), MODIS detections are much reduced, while the higher sensitivity of VIIRS reveals fire activity for an additional two months, including at night. Some of the VIIRS detections can be attributed to industrial fires or wildfires too small to be in the ALVD perimeter dataset. Finally, the

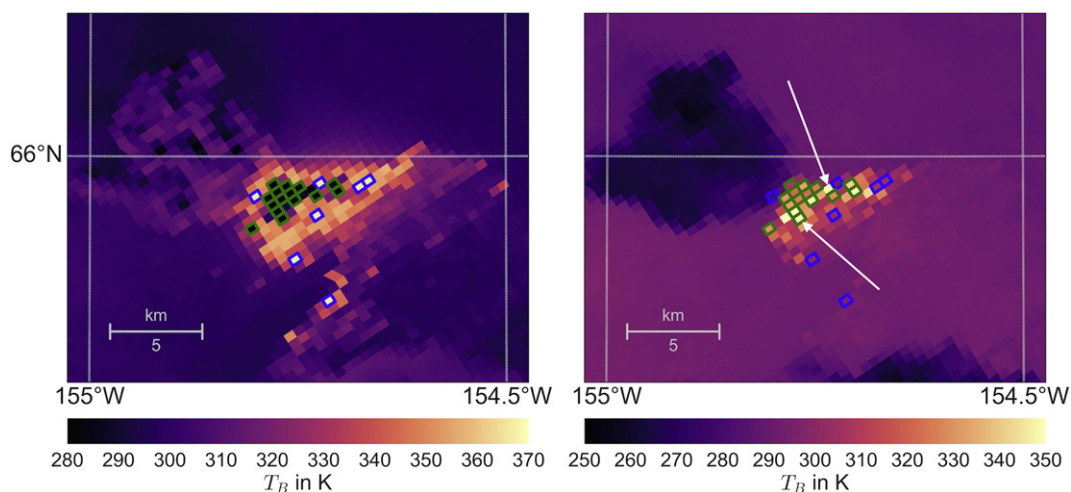


**Fig. 4.** VIIRS I-band pixel anomalies illustrated for a subset of the 2015 Yukon-Koyukuk study area on 2015-07-06. Left: mid-IR brightness temperature (band I4). Right: thermal IR brightness temperature (band I5). Pixels that saturate in I4 appear white (left) and are outlined in blue; the corresponding I5 brightness temperature is within the normal range (nominal quality). Anomalous pixels that appear black (left) and are outlined in green correspond to a “fold-over” of the digital number; all but two of these (white arrows) have nominal quality brightness temperatures in I5.

**Table 5**  
Overall performance of MODIS and VIIRS I-band fire products for detection of 2016 Alaska wildfires.

Fire product	Number of undetected fires	% undetected fires	Size largest undetected fire (ha)	Max. # fire pixels per fire	% fire pixels from oil wells & volcanoes	% unassigned detections
MODIS	70	45%	331	440	0.3	3.3
VIIRS I-band	55	35%	196	1323	3.9	2.0

geographic distribution of fire detections is clustered around the timing of overpasses. For overpasses for which only the swath-edge overlaps with Alaska, fires in some geographical areas are likely to be missed by the sensor. These variations are entirely independent of the processing algorithm and rely only on the orbital and swath characteristics (Fig. 7). The narrower range and timing of potential overpass times of VIIRS compared to MODIS can in some cases lead to a short-lived fire receiving more MODIS than VIIRS I-band detections.

### 6.2. VIIRS I-band Fire Detection Algorithm for High Latitudes (VIFDAHL)

We validated VIFDAHL using near-simultaneous Landsat scenes listed in Table 3. For the Willow study area, on June 15, 2015 and the Eagle study area on May 27, 2015, the corresponding Landsat scenes were acquired within 9 and 2 min, respectively, of the VIIRS granule. For the Yukon-Koyukuk study area, this lapse is approximately 1 min. Spatially, VIFDAHL detections show an excellent match with Landsat detections. There is no obvious co-registration error between the Landsat and the VIIRS footprints (Fig. 8a and b show close-up imagery).

In freshly burned areas, which contain smoldering and residual flaming fires, we tend to find detections of low-intensity fire. There is no false signal from riverbanks or old fire scars in any test scene, but there are areas where sporadic Landsat fire detections are present without a corresponding VIFDAHL detection. For the Willow case ( $N = 22$  VIIRS detections), the mean Landsat fire pixel count for a VIFDAHL high-intensity pixel is 18.7 (standard deviation: 12.5), and for a low-intensity pixel 12.7 (std: 19.1). For the Eagle case, we identify 9 fire pixels (8 high-intensity, 1 low-intensity). High-intensity VIFDAHL pixels contain higher numbers of Landsat fire pixel than low-intensity fire detections (Table 6). Landsat pixel counts were not carried out for the Northern Koyukuk case, as the time lapse between Landsat 8 and VIIRS overpass was too great and the fires too fast-moving for the result to be meaningful.

VIFDAHL detections were compared with the global VIIRS I-band (375 m) product for all four study areas (Table 6). Overall, high-intensity VIFDAHL detections closely approximate VIIRS I-band fire pixels (Figs. 8a–b, 9b–d). In addition, VIFDAHL delivers a second set of detections of less intense fire, predominantly in areas that contain Landsat 8 fire detections, but no VIIRS I-band or high-intensity VIFDAHL

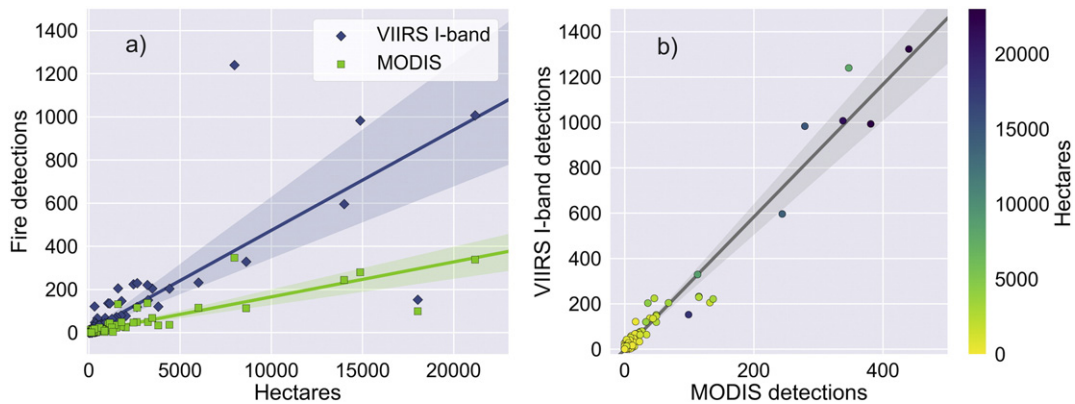


**Fig. 5.** Global VIIRS I-band (375 m) vs. MODIS (both Terra and Aqua) fire detection counts. A point represents a fire event of the Alaska Large Fire Database for 2016 (155 fire events). a) Number of fire detections vs. fire area. Linear regression yields an average of 1.6 MODIS detections ( $r^2 = 0.84$ ) and 4.7 VIIRS I-band detections ( $r^2 = 0.78$ ) per  $\text{km}^2$  of fire area. b) There is a strongly linear relationship between the number of VIIRS I-band and MODIS detections for each fire ( $r^2 = 0.96$ , slope = 2.9). The 95% confidence intervals are indicated as shaded.

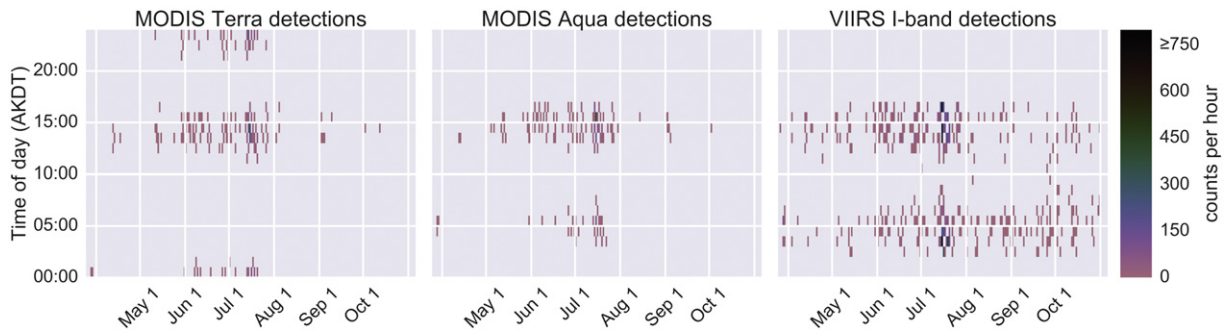


**Fig. 6.** Hourly detection counts across the Alaska 2016 fire season for global fire products: MODIS Terra, MODIS Aqua and VIIRS I-band (375 m) detections. Hourly counts only show one spike in July and are otherwise low ( $<100$ ). MODIS detections generally fall off in August, while the higher sensitivity of VIIRS reveals fire activity for an additional two months. The banding of detection timing is due to the temporal grouping of satellite overpasses. For MODIS Terra, mid-day/early afternoon overpasses occur on a descending node, and late evening overpasses on an ascending node; for Modis Aqua and VIIRS on Suomi NPP, the early afternoon overpasses occur on an ascending node and the early morning overpasses on a descending node. (All times of day are in Alaska Daylight Time.)

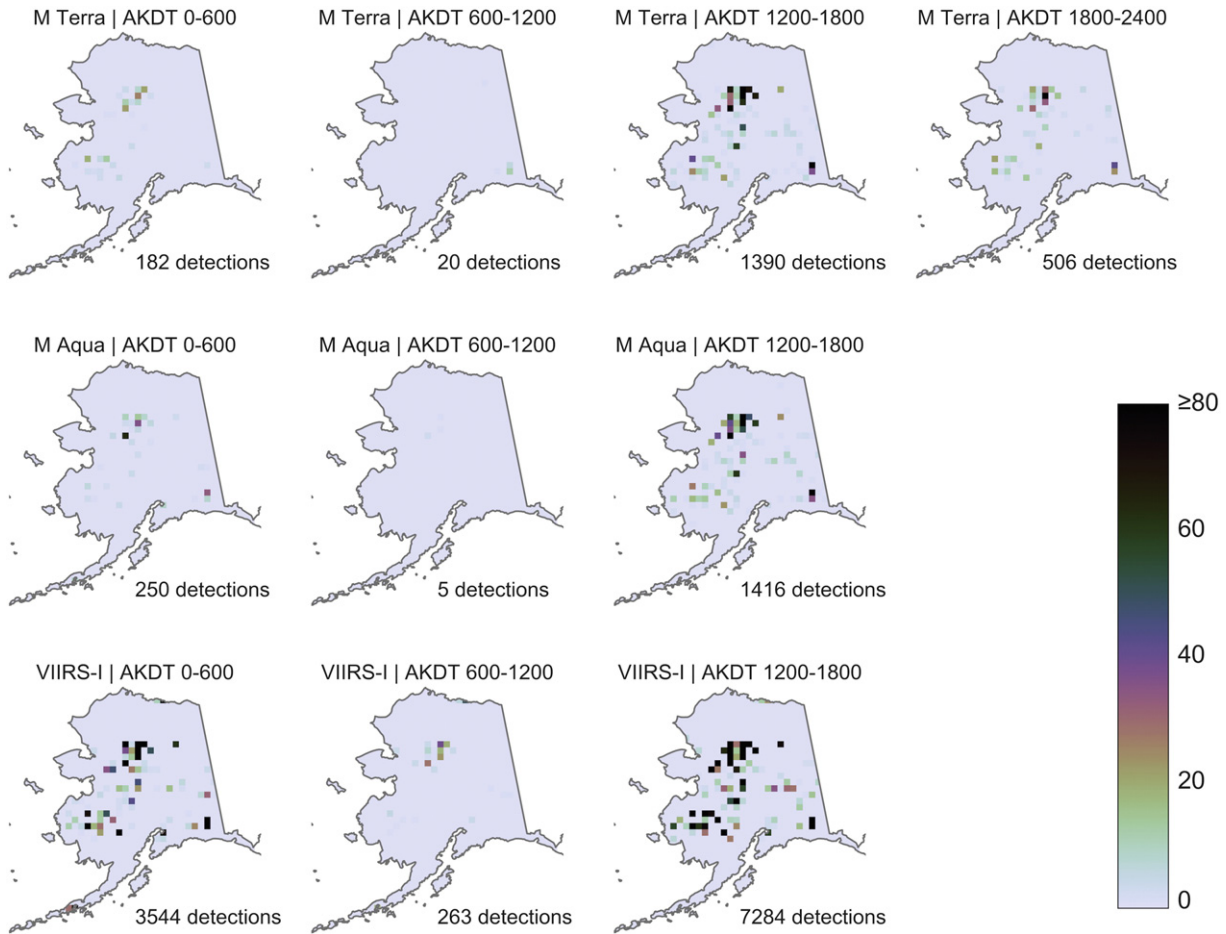


**Fig. 7.** Spatio-temporal distribution of fire detections from global active fire products, in Alaska Daylight Time, during the 2016 fire season, aggregated to a 25 by 25 km grid. Top row: MODIS Terra. Middle row: MODIS Aqua. Bottom row: VIIRS on SUOMI NPP, I-band product. There are no fire detections for MODIS Aqua or NPP/VIIRS during the 18:00 to 24:00 time slot.

detections. Not all low-intensity VIFDAHL detections contain Landsat 8 detections. While it is not at present possible to exclude that VIFDAHL may falsely detect areas where a fresh fire scar is still hot, but extinguished, possible alternative reasons for the absence of Landsat detections are: the shorter wavelength of Landsat's SWIR bands, which is more affected by smoke and clouds, and requires higher temperatures to activate; and the time lapse between VIIRS and Landsat overpasses. Moreover, some high-intensity VIFDAHL and VIIRS I-band fire pixels also correspond to zero Landsat 8 fire pixel counts.

A source of potentially false VIFDAHL detections can be seen in areas with high-intensity fire and large amounts of smoke or clouds. Such an example is visible in the two westernmost fires in Fig. 9a, as a halo of detections around the area that certainly contains fire.

In the two smaller test scenes, Eagle and Willow, where fire was burning with less intensity and/or was more heavily suppressed, VIFDAHL yields between 30 and 50% more detections than the global VIIRS I-band dataset. For the two large-scale extended burn events of the 2015 Yukon Koyukuk and the 2016 Northern Koyukuk study area, we count approximately 90% more VIFDAHL than VIIRS I-band detections, some of which capturing residual fire as mapped by Landsat, some due to the halo-effect around smoke plumes.

## 7. Discussion and conclusions

Based on the analysis of the 2016 Alaska fire season, the 375 m global VIIRS I-band fire product performs better than the MODIS product in Alaska, mainly due to the higher spatial resolution, providing about three times the number of fire detections for an average fire than the MODIS-based product. A VIIRS pixel's footprint on the ground is by

about a factor of 7 smaller than a MODIS pixel, at nadir. As only a small fraction of this footprint is on fire, the non-burning fraction can vary widely. Even though an investigation of sub-pixel active fire area is beyond the scope of this study, we can note that Kasischke et al. (2010) determine the fraction of the area covered by ALFD polygons that was unburned. They find an unburned fraction of about 20% for the extreme fire year of 2004, and much higher values of up to 70% in small fire years. We would therefore not expect the number of detections to grow proportionally to the pixel area.

We aimed to provide fire managers and other data users in the high northern latitudes with criteria to evaluate and understand the spatio-temporal patterns contained in the global fire detection data that are centrally available from MODIS and VIIRS-based products. Due to the timing of satellite overpasses, late evening detections come exclusively from MODIS Terra, while VIIRS on Suomi NPP delivers a much larger number of early morning detections than either of the MODIS sensors. Fire management service briefings (timed typically early morning, and again in the late afternoon) should rely on detections from the core time of overhead passes (approx. 11:30 to 15:30 AKDT for daytime detections, and 21:30 to 1:30 AKDT for MODIS Terra or 2:00 to 6:00 AKDT for MODIS Aqua or VIIRS for nighttime detections) to maximize the area from which detections could potentially originate.

VIFDAHL is easy to implement and computationally light-weight, as it uses simple thresholds on bands and band combinations, tuned for Alaskan boreal forest fires. The Alaska-specific approach with VIFDAHL was able to detect more low-intensity fire pixels than the global operational VIIRS I-band products. This is of interest for mapping areas that are most likely to pose a residual hazard and need to be monitored for any renewed need of fire suppression activity. While VIFDAHL appears

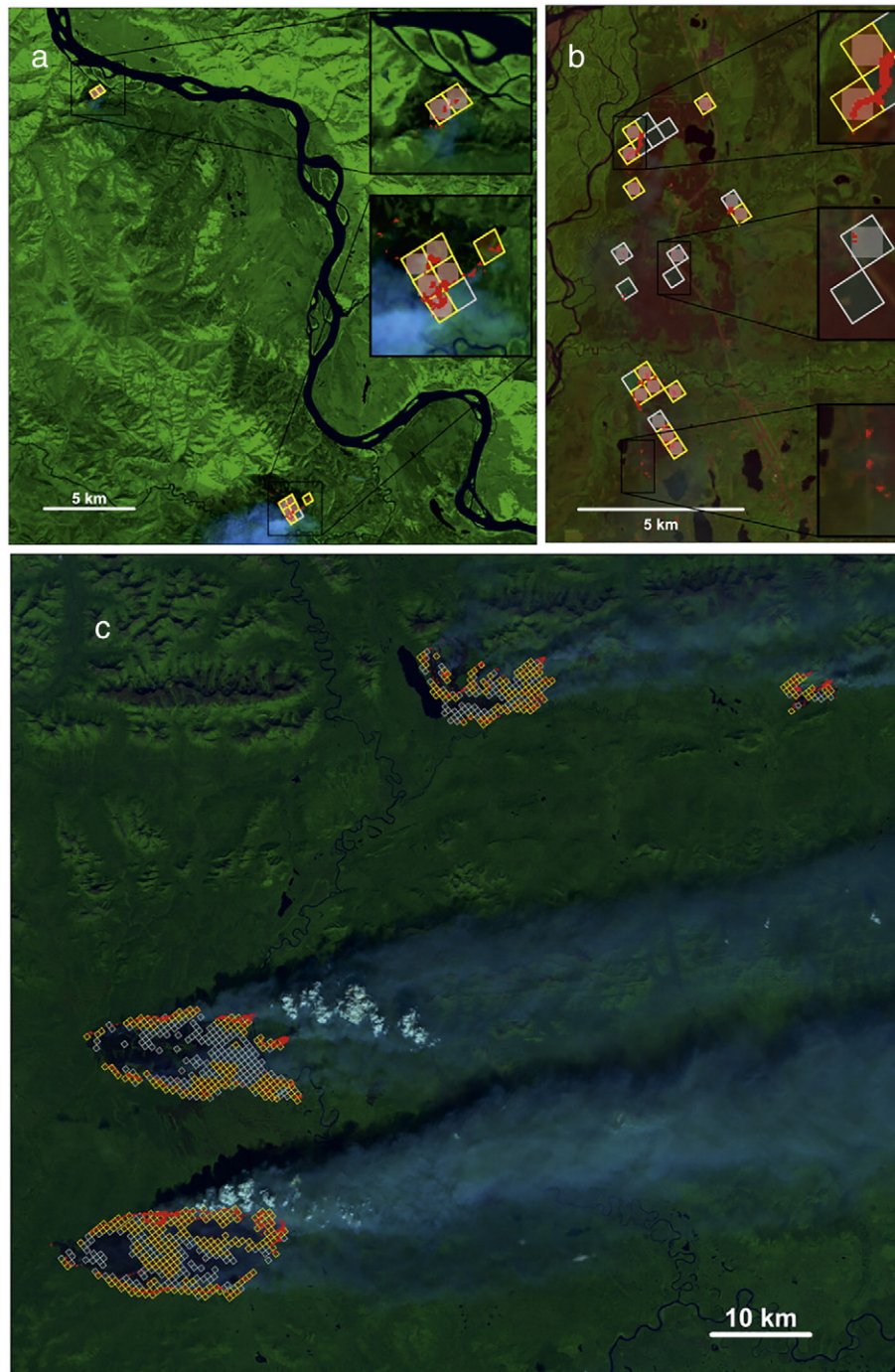


**Fig. 8.** Overview of three study areas with VIFDAHL fire detections outlined in yellow (high-intensity active fire) and grey (low-intensity fire), on a background of near-simultaneous Landsat 7-5-3 false color RGB composite with Landsat fire detections overlaid in red. a) Eagle, 2016-05-27, central latitude 64.0°N, longitude 141.4°W. b) Willow, 2015-06-15, central latitude 61.8°N, longitude 151.1°W. c) Northern Koyukuk 2016-07-15, central latitude 66.9°N, longitude 153.1°W. In a) and b), VIFDAHL fire pixels that are also detected by the global VIIRS 375 m I-band product are shaded.

**Table 6**

Comparison of VIFDAHL with the global VIIRS I-band product and with Landsat 8 fire detections.

Study area	VIIRS I-band (global product) detections	VIFDAHL high-intensity fire detections	Landsat 8 detections per VIFDAHL high intensity pixel mean (std)	VIFDAHL low-intensity fire detections	Landsat 8 detections per VIFDAHL low-intensity pixel: mean (std)
Willow 2015	15	11	18.7 (12.5)	11	12.7 (19.1)
Eagle 2015	7	8	28.3 (19.9)	1	2 (n/a)
Yukon-Koyukuk 2015	633	745	14.6 (30.5)	325	7.9 (21.1)
Northern Koyukuk 2016, scene 1	440	458	n/a	388	n/a
Northern Koyukuk 2016, scene 2	1006	1143	n/a	791	n/a

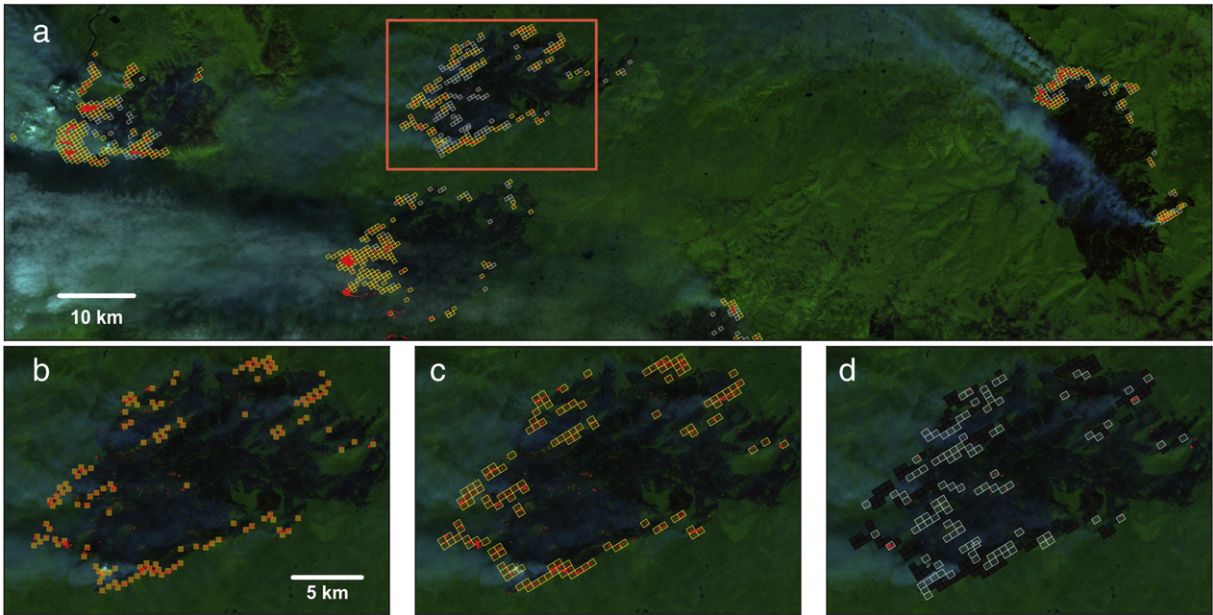


**Fig. 9.** Overview and zoom into 2015 Yukon-Koyukuk study area, 2015-07-06, central latitude 65.9°N, longitude 152.7°W. Fire detection from a single VIIRS scene at 12:58 local time (AKDT) on top of a Landsat 8 bands 7-5-3 false color RGB composite, with Landsat fire detections marked in red. a) Entire study area, VIFDAHL detections, zoomed-in area outlined in red. b) Fire detections from the global VIIRS I-band product. c) VIFDAHL high-intensity detections. d) VIFDAHL low-intensity detections, with the locations of high intensity detections masked out in black for greater visual clarity.

to successfully avoid false detections from river banks or old fire scars, future work should look more closely into errors of commission, informed by experience gathered in operational use. Local VIFDAHL processing enables enhanced geo-location, which can be used for superior fire progression mapping (Fig. 10). Another application would be and stacking of repeated VIFDAHL detections in the same location to be used to estimate fire residence time, with potential links to fire severity. Further study is desirable with the objective to test the algorithm on the Canadian and Eurasian boreal forests.

**Acknowledgements**

This research was supported by NASA Headquarters under the NASA Earth and Space Science Fellowship Program – Grant NNX13AN90H. This research was supported in part by a UAF Center for Global Change Student Research Grant with funds from the Cooperative Institute for Alaska Research, and funding support from UAFs

College of Natural Science and Mathematics. C Waigl is grateful to Alison York, Randi Jandt and Robert Ziel from the Alaska Fire Science Consortium as well as Evan Ellicott for many fruitful discussions, and to Wilfrid Schroeder for providing us with VIIRS I-band 375 m active fire data for the 2015 study areas. We thank the anonymous reviewers for their thoughtful critique, which improved the manuscript substantially.

We acknowledge the use of data and imagery from LANCE FIRMS operated by the NASA/GSFC/Earth Science Data and Information System (ESDIS) with funding provided by NASA/HQ. Landsat 8 data was available from the US Geological Survey.

**References**

Andreae, M.O., Merlet, P., 2001. Emission of trace gases and aerosols from biomass burning. *Glob. Biogeochem. Cycles* 15 (4):955–966. <http://dx.doi.org/10.1029/2000GB001382>.  
 Cao, C., Luccia, F.J.D., Xiong, X., Wolfe, R., Weng, F., 2014. Early on-orbit performance of the Visible Infrared Imaging Radiometer Suite onboard the Suomi National Polar-Orbiting

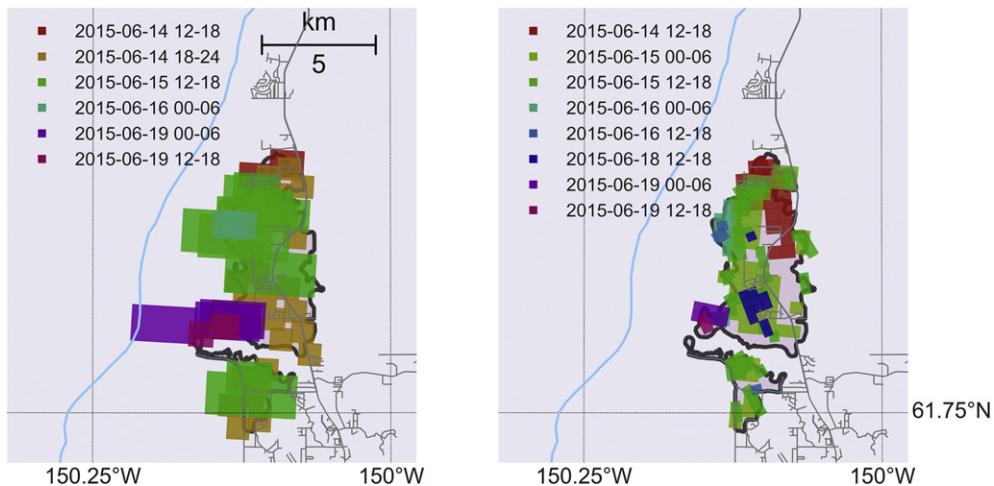


**Fig. 10.** Willow study area, fire progression in 6-hour intervals. Roads, the Susitna River, and the official AICC fire perimeter are outlined. Left: MODIS active fires (pixel dimensions, but not orientation, are realistic from data). Right: VIFDAHL. A complete dataset of the global VIIRS I-band detections was not available for this 2015 fire.

- Partnership (S-NPP) satellite. *IEEE Trans. Geosci. Remote Sens.* 52 (2):1142–1156. <http://dx.doi.org/10.1109/TGRS.2013.2247768>.
- Collins, M., Knutti, R., Arblaster, J., Dufresne, J.-L., Fichet, T., Friedlingstein, P., Gao, X., Gutowski, W.J., Johns, T., Krinner, G., Shongwe, M., Tebaldi, C., Weaver, A.J., Wehner, M., 2013. Long-term climate change: projections, commitments and irreversibility. In: Stocker, F.T., Qin, D., Plattner, G.-K., Tignor, M., Allen, S.K., Boschung, J., Nauels, A., Xia, Y., Bex, V., Midgley, P.M. (Eds.), *Climate Change 2013: The Physical Science Basis. Contributions of Working Group I to the Fifth Assessment Report of the Intergovernmental Panel on Climate Change*. Cambridge University Press, Cambridge, United Kingdom, pp. 1029–1136.
- Csiszar, I.A., Morissette, J.T., Giglio, L., 2006. Validation of active fire detection from moderate-resolution satellite sensors: the MODIS example in northern Eurasia. *IEEE Trans. Geosci. Remote Sens.* 44 (7):1757–1764. <http://dx.doi.org/10.1109/TGRS.2006.875941>.
- Csiszar, I., Schroeder, W., Giglio, L., Ellicott, E., Vadrevu, K.P., Justice, C.O., Wind, B., 2014. Active fires from the Suomi NPP Visible Infrared Imaging Radiometer Suite: product status and first evaluation results. *J. Geophys. Res. Atmos.* 119 (2). <http://dx.doi.org/10.1002/2013JD020453>.
- Dozier, J., 1981. A method for satellite identification of surface temperature fields of subpixel resolution. *Remote Sens. Environ.* 11:221–229. [http://dx.doi.org/10.1016/0034-4257\(81\)90021-3](http://dx.doi.org/10.1016/0034-4257(81)90021-3).
- Genet, H., McGuire, A.D., Barrett, K., Breen, A., Euskirchen, E.S., Johnstone, J.F., ... Yuan, F., 2013. Modeling the effects of fire severity and climate warming on active layer thickness and soil carbon storage of black spruce forests across the landscape in interior Alaska. *Environ. Res. Lett.* 8 (4):045016. <http://dx.doi.org/10.1088/1748-9326/8/4/045016>.
- Giglio, L., Kendall, J.D., Justice, C.O., 1999. Evaluation of global fire detection algorithms using simulated AVHRR infrared data. *Int. J. Remote Sens.* 20 (10):1947–1985. <http://dx.doi.org/10.1080/014311699212290>.
- Giglio, L., Desloires, J., Justice, C.O., Kaufman, Y.J., 2003. An enhanced contextual fire detection algorithm for MODIS. *Remote Sens. Environ.* 87 (2–3):273–282. [http://dx.doi.org/10.1016/S0034-4257\(03\)00184-6](http://dx.doi.org/10.1016/S0034-4257(03)00184-6).
- Giglio, L., Schroeder, W., Justice, C.O., 2016. The collection 6 MODIS active fire detection algorithm and fire products. *Remote Sens. Environ.* 178:31–41. <http://dx.doi.org/10.1016/j.rse.2016.02.054>.
- Grell, G., Freitas, S.R., Stuefer, M., Fast, J., 2011. Inclusion of biomass burning in WRF-Chem: impact of wildfires on weather forecasts. *Atmos. Chem. Phys.* 11 (11): 5289–5303. <http://dx.doi.org/10.5194/acp-11-5289-2011>.
- Ichoku, C., Kahn, R., Chin, M., 2012. Satellite contributions to the quantitative characterization of biomass burning for climate modeling. *Atmos. Res.* 111:1–28. <http://dx.doi.org/10.1016/j.atmosres.2012.03.007>.
- Johnstone, J.F., Hollingsworth, T.N., Chapin, F.S., Mack, M.C., 2010. Changes in fire regime break the legacy lock on successional trajectories in Alaskan boreal forest. *Glob. Chang. Biol.* 16 (4):1281–1295. <http://dx.doi.org/10.1111/j.1365-2486.2009.02051.x>.
- Justice, C., Giglio, L., Korontzi, S., Owens, J., Morissette, J., Roy, D., ... Kaufman, Y., 2002. The MODIS fire products. *Remote Sens. Environ.* 83 (1–2):244–262. [http://dx.doi.org/10.1016/S0034-4257\(02\)00076-7](http://dx.doi.org/10.1016/S0034-4257(02)00076-7).
- Kasischke, E.S., Hoy, E.E., 2012. Controls on carbon consumption during Alaskan wildland fires. *Glob. Chang. Biol.* 18 (2):685–699. <http://dx.doi.org/10.1111/j.1365-2486.2011.02573.x>.
- Kasischke, E.S., Turetsky, M.R., 2006. Recent changes in the fire regime across the North American boreal region—spatial and temporal patterns of burning across Canada and Alaska. *Geophys. Res. Lett.* 33 (9):L09703. <http://dx.doi.org/10.1029/2006GL025677>.
- Kasischke, E.S., Williams, D., Barry, D., 2002. Analysis of the patterns of large fires in the boreal forest region of Alaska. *Int. J. Wildland Fire* 11 (2), 131–144.
- Kasischke, E.S., Hyer, E.J., Novelli, P.C., Bruhwiler, L.P., French, N.H.F., Sukhinin, A.I., ... Stocks, B.J., 2005. Influences of boreal fire emissions on Northern Hemisphere atmospheric carbon and carbon monoxide. *Glob. Biogeochem. Cycles* 19 (1):GB1012. <http://dx.doi.org/10.1029/2004GB002300>.
- Kasischke, E.S., Verbyla, D.L., Rupp, T.S., McGuire, A., Murphy, K.A., Jandt, R., ... Turetsky, M.R., 2010. Alaska's changing fire regime: implications for the vulnerability of its boreal forests. *Can. J. For. Res.* 40 (7), 1313–1324.
- Kaufman, Y.J., Justice, C.O., Flynn, L.P., Kendall, J.D., Prins, E.M., Giglio, L., ... Setzer, A.W., 1998. Potential global fire monitoring from EOS-MODIS. *J. Geophys. Res.* 103 (D24): 32,215–32,238. <http://dx.doi.org/10.1029/98JD01644>.
- Li, Z., Nadon, S., Cihlar, J., 2000a. Satellite-based detection of Canadian boreal forest fires: development and application of the algorithm. *Int. J. Remote Sens.* 21 (16): 3057–3069. <http://dx.doi.org/10.1080/01431160050144956>.
- Li, Z., Kaufman, Y.J., Ichoku, C., Fraser, R., Trishchenko, A., Giglio, L., ... Yu, X., 2000b. A Review of AVHRR-based Active Fire Detection Algorithms: Principles, Limitations, and Recommendations. Canada Cent. Remote Sens., Ottawa, Canada Retrieved from. [http://www.fao.org/GTOS/gofc-gold/docs/fire\\_ov.pdf](http://www.fao.org/GTOS/gofc-gold/docs/fire_ov.pdf).
- Liang, C.K., Mills, S., Hauss, B.I., Miller, S.D., 2014. Improved VIIRS day/night band imagery with near-constant contrast. *IEEE Trans. Geosci. Remote Sens.* 52 (11):6964–6971. <http://dx.doi.org/10.1109/TGRS.2014.2306132>.
- Matson, M., Dozier, J., 1981. Identification of subresolution high temperature sources using a thermal IR sensor. *Photogramm. Eng. Remote. Sens.* 47 (9), 1311–1318.
- Menzel, W.P., Prins, E.M., 1996. Monitoring biomass burning with the new generation of geostationary satellites. *Biomass Burning Glob. Chang.* 1, 56–64.
- Pfister, G., Hess, P.G., Emmons, L.K., Lamarque, J.-F., Wiedinmyer, C., Edwards, D.P., ... Sachse, G.W., 2005. Quantifying CO emissions from the 2004 Alaskan wildfires using MOPITT CO data. *Geophys. Res. Lett.* 32 (11). <http://dx.doi.org/10.1029/2005GL022995>.
- Pfister, G.G., Emmons, L.K., Hess, P.G., Honrath, R., Lamarque, J.F., Val Martin, M., ... Holloway, J.S., 2006. Ozone production from the 2004 North American boreal fires. *J. Geophys. Res.* 111, D24507.
- Pfister, G.G., Hess, P.G., Emmons, L.K., Rasch, P.J., Vitt, F.M., 2008. Impact of the summer 2004 Alaska fires on top of the atmosphere clear-sky radiation fluxes. *J. Geophys. Res. Atmos.* 113 (D2). <http://dx.doi.org/10.1029/2007JD008797>.
- Polivka, T.N., Wang, J., Ellison, L.T., Hyer, E.J., Ichoku, 2016. Improving nocturnal fire detection with the VIIRS day-night band. *IEEE Trans. Geosci. Remote Sens.* 54 (9). <http://dx.doi.org/10.1109/TGRS.2016.2566665>.
- Prins, E.M., Menzel, W.P., 1994. Trends in South American biomass burning detected with the GOES visible infrared spin scan radiometer atmospheric sounder from 1983 to 1991. *J. Geophys. Res. Atmos.* 99 (D8):16719–16735. <http://dx.doi.org/10.1029/94JD01208>.
- Prins, E., Schmidt, C., 2001. GOES burns bright. *Geospatial Solutions* 11 (7), 33.
- Randerson, J.T., Liu, H., Flanner, M.G., Chambers, S.D., Jin, Y., Hess, P.G., ... Zender, C.S., 2006. The impact of boreal forest fire on climate warming. *Science* 314 (5802):1130–1132. <http://dx.doi.org/10.1126/science.1132075>.
- Roman, J., 2015. The year in wildfire. *NFPA J.* 2015 (Nov–Dec) Retrieved from. <http://www.nfpa.org/news-and-research/publications/nfpa-journal/2015/november-december-2015/features/the-year-in-wildfire>.
- Schroeder, W., Prins, E., Giglio, L., Csiszar, I., Schmidt, C., Morissette, J., Morton, D., 2008. Validation of GOES and MODIS active fire detection products using ASTER and ETM+ data. *Remote Sens. Environ.* 112 (5):2711–2726. <http://dx.doi.org/10.1016/j.rse.2008.01.005>.
- Schroeder, W., Oliva, P., Giglio, L., Csiszar, I.A., 2014. The new VIIRS 375 m active fire detection data product: algorithm description and initial assessment. *Remote Sens. Environ.* 143:85–96. <http://dx.doi.org/10.1016/j.rse.2013.12.008>.
- Schroeder, W., Oliva, P., Giglio, L., Quayle, B., Lorenz, E., Morelli, F., 2016. Active fire detection using Landsat-8/OLI data. *Remote Sens. Environ.* 185, 210–220.
- Soja, A.J., Tchebakova, N.M., French, N.H.F., Flannigan, M.D., Shugart, H.H., Stocks, B.J., ... Stackhouse Jr., P.W., 2007. Climate-induced boreal forest change: predictions versus current observations. *Glob. Planet. Chang.* 56 (3–4):274–296. <http://dx.doi.org/10.1016/j.gloplacha.2006.07.028>.
- Stevens, E., 2014. Joint Polar Satellite Systems (JPSS) Common Data Format Control Book – External - Volume III - SDR/TDR Formats (No. 474-00001-03-B0123). GSFC Retrieved from. [http://npp.gsfc.nasa.gov/sciencedocuments/2014-11/474-00001-03\\_JPSS-CDFCB-X-Vol-III\\_0124C.pdf](http://npp.gsfc.nasa.gov/sciencedocuments/2014-11/474-00001-03_JPSS-CDFCB-X-Vol-III_0124C.pdf).